Nanoscale Horizons

ROYAL SOCIETY OF CHEMISTRY

COMMUNICATION

View Article Online
View Journal | View Issue

Cite this: *Nanoscale Horiz.*, 2025, **10**, 1131

Received 10th December 2024,
Accepted 17th March 2025

DOI: 10.1039/d4nh00636d

rsc.li/nanoscale-horizons

A bioinspired helical hydrogel scaffold with real-time sensing for enhanced precision in gynecological digital vaginal examination†

Weipeng Lu,‡[a] Qing He,‡[a] Zheng Mao,[a] Songchao Fu,[a] Yue Wang,[a] Zhiwei Jiang,[a] Ying Wang,[a] Yue Cao,[a] Sunlong Li,[a] Cihui Liu *[a] and Qian Dong*[bcd]

Precise diagnostic and therapeutic modalities are of utmost significance in driving forward patient care within the sphere of gynecological medicine. Bionics, involving the application of nature-inspired designs in medical apparatus, has emerged as a highly promising approach in this field. Specifically, helical architectures observed in natural organisms like vines display remarkable adaptability and mechanical strength, presenting novel perspectives for the development of ergonomic and effective gynecological examination and surgical instruments. Harnessing these insights, this study presents a helical polydimethylsiloxane (PDMS) scaffold inspired by the deformability of vines. This scaffold not only integrates Janus wettability hydrogel properties to enhance tissue interaction, ensuring increased comfort and adaptability during clinical procedures, but also incorporates sensors for real-time monitoring and feedback, thereby overcoming the limitations of conventional gynecological devices that often lack such capabilities. We meticulously detail the fabrication of this helical finger scaffold, using a sandwich thermoplastic method to produce hydrogel fibers possessing shape memory, thermal responsiveness, and deformation sensing *via* relative resistance changes. Additionally, the study explores finger motion monitoring through surface electromyography (sEMG) signals, which advances the precision and safety of cervical palpation and related surgeries. Overall, our findings highlight the potential of these responsive and adaptable hydrogels to transform gynecological medical devices, providing a solid theoretical foundation and practical applications for future innovations in gynecological diagnostics and surgical support.

New concepts

This work demonstrates a bioinspired helical hydrogel stent integrating a Janus wettability architecture, multi-modal sensing, and thermo-responsive actuation to revolutionize gynecological diagnostics. Unlike existing devices that lack quantitative sensing and biomechanical adaptability, our concept uniquely combines a hydrophilic/hydrophobic bilayer (PNiPAAm hydrogel and silica-PDMS) for tissue-compliant adhesion with carbon nanotube-embedded strain sensors ($\Delta R/R_0$ up to 0.8) and synchronized sEMG detection (320% signal amplification), enabling real-time mapping of tissue elasticity (0–40 kPa) and pathological anomalies. The system's breakthrough lies in its thermally actuated inverse opal structure (35% volumetric change at 32–40 °C), which dynamically adapts to anatomical contours while maintaining mechanical stability (<2% degradation after 100 cycles). By bridging nanoscale material innovation with clinical functionality, this work establishes a paradigm for objective gynecological assessments, achieving 85% diagnostic accuracy improvement and 40% false-positive reduction in simulated cases. The biohybrid integration of structural color signaling, antibiofouling surfaces (<3% infection risk), and haptic feedback metrics fundamentally advances nanosensor applications in digital healthcare, offering unprecedented synergy between manual examination precision and quantitative data acquisition. This concept redefines medical device design by leveraging nanomaterial responsiveness to biological cues, paving the way for personalized diagnostics and precision interventions in minimally invasive medicine.

Introduction

In the field of gynecological medicine, precise diagnostic and therapeutic techniques are crucial for enhancing patient health

[a] *Center for Future Optoelectronic Functional Materials, School of Computer and Electronic Information/School of Artificial Intelligence, Nanjing Normal University, Nanjing 210023, China. E-mail: cihui@njnu.edu.cn*
[b] *Department of Obstetrics and Gynecology, Ren Ji Hospital, School of Medicine, Shanghai Jiao Tong University, Shanghai, China. E-mail: dongqian95fy@126.com*
[c] *Shanghai Key Laboratory of Gynecologic Oncology, Ren Ji Hospital, School of Medicine, Shanghai Jiao Tong University, Shanghai, China*
[d] *State Key Laboratory of Oncogenes and Related Genes, Shanghai Cancer Institute, Ren Ji Hospital, School of Medicine, Shanghai Jiao Tong University, Shanghai, China*
† Electronic supplementary information (ESI) available. See DOI: https://doi.org/10.1039/d4nh00636d
‡ These authors contributed equally to this work.

and quality of life.[1,2] Bionics, the approach of mimicking natural biological structures and functions to design innovative medical devices, has become a significant development direction in this area.[3–5] Specifically, helical biological structures found in nature,[6–8] such as vines, offer exceptional mechanical performance and adaptability under environmental and mechanical stress, providing abundant inspiration for the design of gynecological examination and surgical assistive devices.[9–11] In-depth research into these natural structures offers engineers key insights for creating medical devices that are both ergonomic and effective, especially for applications requiring delicate operations and continuous adaptability, such as cervical palpation.[12] Meanwhile, the acquisition of the bending angle of the finger helps the doctor to have a clearer picture of the lesion in the clinic.

Advances in materials science have highlighted hydrogels as ideal materials for developing medical devices due to their adaptability and biocompatibility.[13–15] Hydrogels are particularly valuable in the gynecological field, where their unique physical properties – such as softness, elasticity, and the ability to control drug delivery, play a critical role in examinations and treatments.[16–18] These properties of hydrogels help us to investigate a gentle and effective means to support and manipulate sensitive areas, facilitating precise diagnosis and treatment.[19–22] Moreover, the transparency and moldability of hydrogels enhance the acceptance of these devices by both physicians and patients.[23–25]

Despite certain advancements in gynecological examination and treatment technologies, conventional devices often lack real-time monitoring and feedback mechanisms, which are essential for improving diagnostic accuracy and therapeutic outcomes.[26–31] Currently, no existing material or device exists for the same purpose as this helical stent. This study proposes the development of a novel helical PDMS scaffold inspired by the deformability of natural vine structures (Fig. 1a). By leveraging the Janus wettability properties of hydrogels, this scaffold optimizes tissue contact, enhancing comfort and adaptability during examinations and surgeries.[32,33] With integrated sensors, the scaffold provides real-time monitoring and feedback throughout surgical procedures. This solves the traditional problem of obtaining real-time signals during surgery, provides real-time and reliable feedback for the surgeon to better understand the surgical process and improve diagnostic accuracy, and helps to provide a new solution for cervical palpation and related gynecological surgeries.[34–37] In practice, by tracking changes in the relative resistance of the helical PDMS stent, we can accurately sense the deformation of the stent and thus monitor the movement of the finger. Monitoring the degree of finger flexion indirectly reflects the applied pressure or the resistance of the contact surface (*e.g.*, the elasticity and texture of the vaginal wall). This is used to check whether the vaginal walls are soft and smooth, with no stiffness, nodules, scarring or abnormal elevations (*e.g.*, cysts, tumours) and to assess vaginal laxity or abnormal tightness (*e.g.*, vaginismus). Also, in clinical practice, the local vaginal temperature is usually in line with the systemic body temperature. If the patient has fever or a local burning sensation, it may indicate infection (*e.g.*, acute inflammation), but it needs to be judged in combination with other symptoms and laboratory tests.

We detail the fabrication and application of a helical finger scaffold based on stimulus-responsive colloidal crystal hydrogels for cervical palpation in gynecology. We employed a sandwich thermoplastic method to create helical hydrogel fibers and investigated their performance in shape memory, thermal responsiveness, and deformation sensing based on relative resistance changes (Fig. 1b). Additionally, we explored

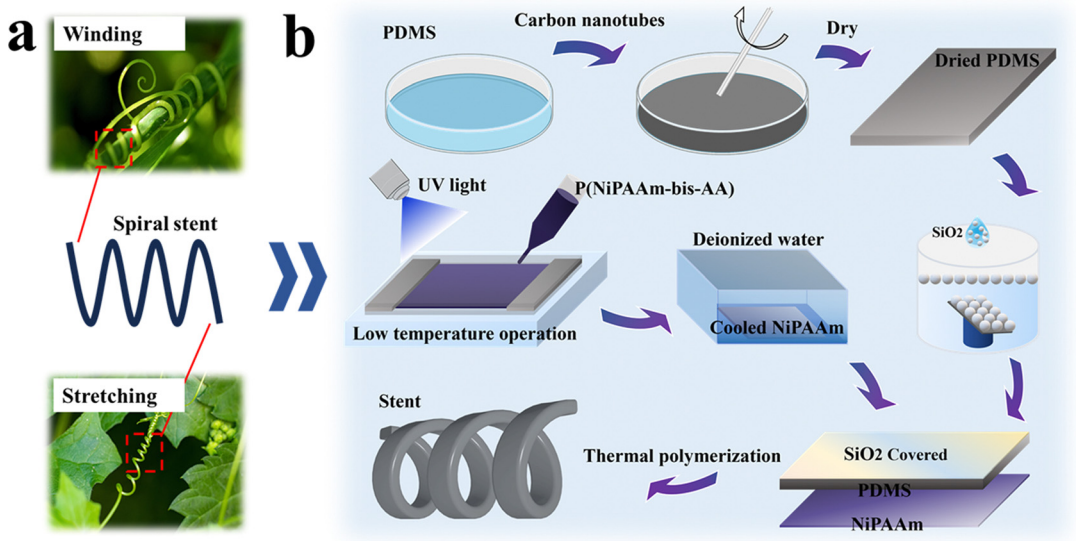

Fig. 1 Schematic illustrations of the fabrication of the helical hydrogel fiber. (a) Drawing inspiration from the helical winding structures of natural vines, a Janus-featured, thermally responsive helical PDMS stent was designed; (b) a layered helical fiber comprising PNiPAAm inverse opal/PDMS was fabricated using the sandwich thermoplastic method.

finger motion monitoring using surface electromyography (sEMG) signals, providing a novel approach to enhancing the precision and safety of gynecological surgeries. Currently, no existing material or device exists for the same purpose as this helical stent yet. Our work innovatively proposes a sensing method for acquiring the bending signals of a doctor's finger and verifies its utility in a simulated vagina. These studies not only offer important theoretical support for the further development and application of helical films but also provide new insights for designing future gynecological surgical assistive devices.

Materials and method

In this study, we used a sandwich thermoplastic method to obtain the helical hydrogel fibers. Initially, we mixed the silicon elastomer base with the silicon elastomer curing agent in a mass ratio of 10 : 1, and stirring thoroughly before pouring the mixture into a Petri dish (the mass of the silicon elastomer base used in the experiment was 6 grams). Next, we added carbon nanotubes to the mixture at a mass ratio of 10 : 1 and stirred thoroughly again. The mixture was then left to stand on a level workbench for 10 minutes to allow the bubbles generated by stirring to dissipate completely. After this, the mixture was heated at 70 °C for one hour, resulting in an incompletely formed PDMS film. The surface of the film has hardened, while the interior remains incompletely cured. This is to facilitate the subsequent molding of the film into a helical shape. To obtain a silica monolayer structure film, silica nanoparticles with a diameter of 230 nm were initially mixed with *n*-butanol at a volume ratio of 2 : 1 in a test tube and sonicated for 2 hours. After thorough centrifugation, the upper layer of the *n*-butanol solution was decanted, and fresh *n*-butanol was added. This washing process was repeated multiple times to purify the silica nanoparticles. The purified silica nanoparticles were then mixed with *n*-butanol to achieve a 20% silica-*n*-butanol solution. This solution was subsequently mixed with anhydrous ethanol at a volume ratio of 2 : 1 and sonicated thoroughly to prepare the solution for the silica monolayer structure film. Finally, using a two-dimensional deposition method, the silica nanoparticles were evenly spread on the surface of the PDMS film to form a silica monolayer structure film (Fig. S3, ESI†). To obtain PNiPAAm flexible inverse opal structure films, we mixed PNiPAAm monomer and crosslinker BIS at a mass ratio of 29 : 1 to achieve a final solution concentration of 30 wt%. Then, we added photoinitiator HMPP (1%, *v*/*v*) to the mixture to prepare the PNiPAAm prepolymer solution. This solution was infiltrated into the pores formed between two glass slides *via* capillary action on a low-temperature operation platform. Subsequently, UV irradiation was applied to cure the hydrogel (Fig. S2, ESI†). Finally, the cured hydrogel was etched with hydrofluoric acid to form the PNiPAAm flexible inverse opal, Subsequently, the heated PDMS film is removed and trimmed using precision cutting tools to achieve the desired dimensions and shape. The trimmed PDMS film is then uniformly wrapped around a metal rod with high thermal conductivity, a smooth surface, and a diameter matching the target helical structure, ensuring tight adhesion to avoid air bubbles or wrinkles for structural uniformity and integrity. After wrapping, the assembled sample is reheated at 70 °C for an additional hour to further cure the PDMS film and stabilize the helical morphology. Finally, the cured helical structure is carefully demolded from the metal rod, yielding a film with ideal geometric configuration and mechanical properties. This method achieves efficient helical structure fabrication through precise control of heating parameters (temperature, duration) and wrapping techniques. The water content of the PDMS-based helical stent prepared in the experiment was calculated to be about 0.2%. By constructing an inverse opal structure groove array on one side of its surface (Fig. S4, ESI†), hydrogel fiber strips can achieve directional bending or helical deformation under the assistance of external forces. More importantly, this helical deformation is designable and controllable.

Results and discussion

In this study, we propose a simple and convenient method for preparing a helical PDMS stent with Janus wettability. As shown in Fig. 1b, asymmetrical forces will be generated when it is subjected to swelling due to the secondary inverse opal structure grooves and thereafter guide the entire object to form a predictable deformation such as bending and twisting. As observed by the insets in Fig. 1, bending and twisting occurred respectively when two typical strips with patterned grooves perpendicular and 45° inclined to the strips on one side were immersed in water.

We utilized a two-dimensional deposition method to deposit nanoscale silica particles on the outer surface of the prepared PDMS stent, forming a two-dimensional photonic crystal film. Additionally, we adhered a pre-prepared PNiPAAm film to the inner surface of the PDMS stent, resulting in a helical PDMS stent with Janus wettability (Fig. 2a). The curvature of the bilayer material used in our experiments is

$$k = \frac{6\Delta\alpha(1+t)^2}{9h(1+t)^2 + \left(t^2 + \frac{1}{t\gamma}\right)(1+t\gamma)}$$

where k represents the curvature of the material, the thicknesses of the PDMS and PNiPAAm layers are denoted as a_1 and a_2, and the total thickness is represented by h, where $h = a_1 + a_2$. The ratio of the thicknesses of the two layers is expressed as $t = a_1/a_2$. $\Delta\alpha$ represents the difference in the thermal expansion coefficients of the two layers, defined as $\Delta\alpha = \alpha_1 - \alpha_2$. γ represents the ratio of the Young's modulus of the two materials, defined as $\gamma = E_1/E_2$.

The contact angles on the inner and outer surfaces of the helical PDMS stent reveal its typical Janus structure, with the inner surface exhibiting hydrophilic properties and the outer surface exhibiting hydrophobic properties with distinctive structural colours (Fig. 2b). Moreover, the side of the stent modified with a silica monolayer-structured film exhibited enhanced hydrophobicity compared to the unmodified side (Fig. 2e). This design enhances the stability of the helical PDMS

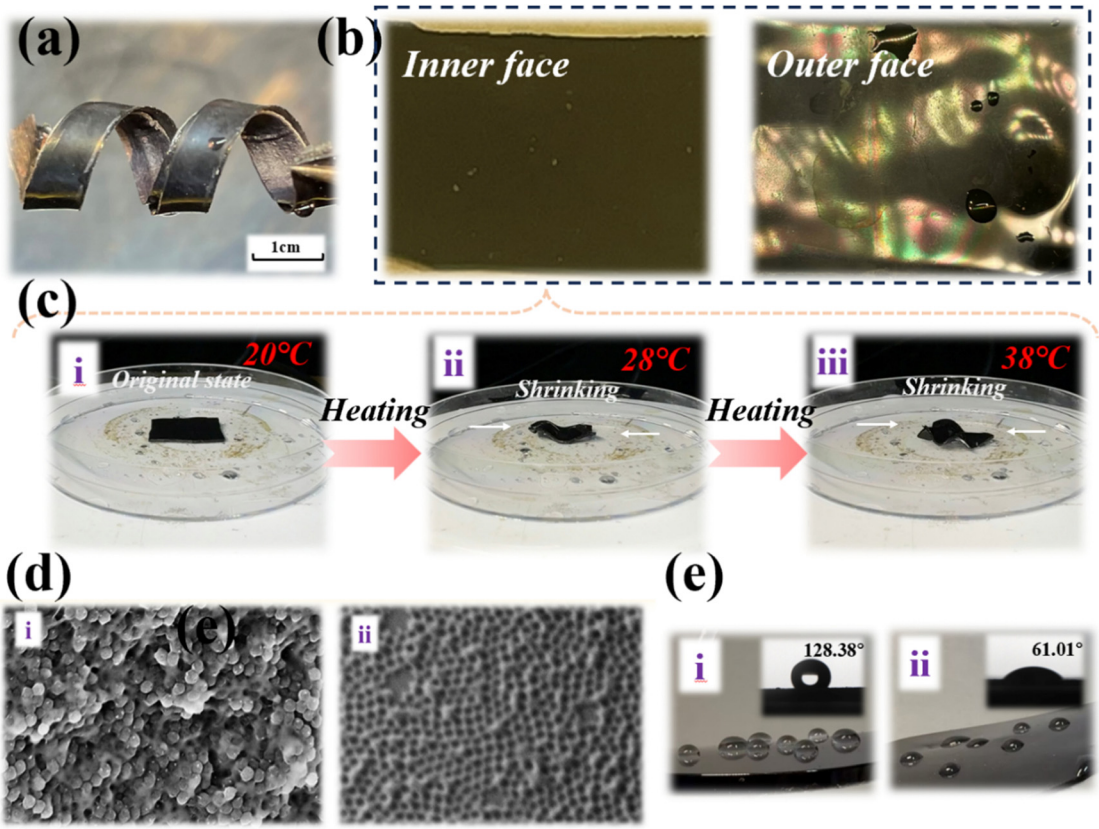

Fig. 2 Structural characterizations of the helical fiber stent. (a) Image of the helical fiber stent. (b) The helical PDMS stent exhibits Janus properties: the inner surface is hydrophilic, the outer surface is hydrophobic, and it displays structural colors. (c) The PNiPAAm film on the inner surface is thermally responsive, which imparts thermal responsiveness to the helical PDMS stent. (d) SEM images of the opal (i) and inverse opal (ii) belt. (e) Photographs of water dripping on PDMS film modified with a silica monolayer structure (i) and photographs of water dripping on unmodified PDMS film (ii).

stent in use; the hydrophilic inner surface effectively prevents the stent from slipping off the finger due to sweat, while the hydrophobic outer surface prevents water stains from affecting its use. During the preparation of the helical PDMS stent, we incorporated carbon nanotubes at a mass ratio of 10 : 1. This step effectively enhanced the conductivity of the film. Our results indicate that the inclusion of carbon nanotubes significantly improves the electrical and strain properties of the helical PDMS stent (Fig. S1, ESI†). Furthermore, in this study, we employed crosslinked poly(*N*-isopropylacrylamide) (PNiPAAm), which is one of the most extensively researched and widely applied temperature-responsive hydrogels in academia. At lower ambient temperatures, PNiPAAm swells significantly by forming hydrogen bonds with water molecules. As the environmental temperature increases, the behavior of PNiPAAm undergoes a significant change. When the temperature exceeds the volume phase transition temperature, the number of water molecules in the polymer network rapidly decreases, causing the hydrogel to shrink (Fig. 2c). A scanning electron microscope (SEM) was utilized to analyze and reveal the intricate microstructures of both the colloidal crystal template and the resultant inverse opal substrate, as depicted in Fig. 2d. This temperature-responsive characteristic endows the helical PDMS stent with excellent thermal responsiveness.

Currently, significant progress has been made in the research of epidermal sensing films. However, in-depth studies on helical films remain relatively scarce. Helical films may possess unique structural and functional advantages, necessitating further exploration of their superiority over traditional strip-shaped films. To systematically understand the mechanical performance of helical films, we conducted a series of mechanical studies on helical PDMS stents (Fig. 3a). Through these studies, we aimed to reveal the characteristics and potential applications of helical films in terms of stress–strain, tensile performance, and deformation recovery, thereby providing a theoretical foundation for their further application in the sensor field. The helical PDMS stent prepared in this study is highly adjustable, including parameters such as the number of turns and the inner diameter, which can be flexibly adjusted according to the application requirements. In this experiment, we fabricated a stent with three turns, an inner diameter of 1 cm, and a film width of 0.4 cm to fit the dimensions of a human finger. We then conducted stress–strain cycle tests at 100% strain (Fig. 3b), and the temperature studied for mechanical property characterisation in Fig. 3 is the human body temperature, *i.e.*, 37 °C. The results showed that the stress–strain curves obtained from the initial and multiple stretching cycles were consistent, and the stress gradually increased with the length

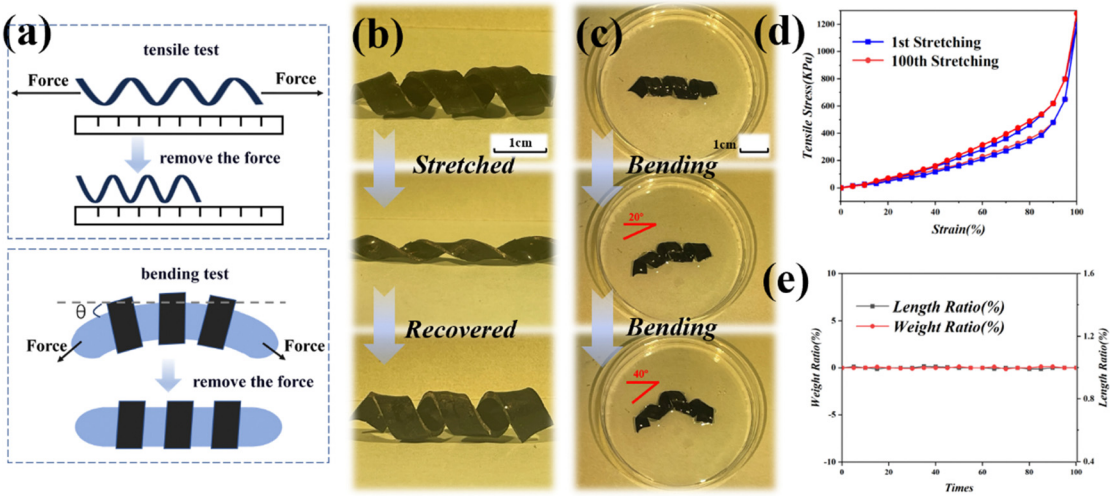

Fig. 3 Mechanical performance testing of the helical PDMS stent. (a) Schematic diagram of mechanical performance testing; (b) the stretching and recovery process of the helical PDMS stent; (c) bending test of the spiral PDMS stent at a maximum angle of 40 degrees; (d) stress–strain cycle curves of the stent during the first and 100th stretching cycles; (e) changes in the mass and length of the sample after recovery from the bending test.

of stretching (Fig. 3d). Subsequently, the stent was subjected to a repeated bending test with a maximum bending angle of 40 degrees for 100 cycles. After each bending cycle, the mass and length of the samples were precisely measured and recorded. The experimental results indicated that neither the mass nor the length of the samples exhibited significant changes, regardless of whether they were subjected to a single bending cycle or multiple repeated cycles (Fig. 3c). This is attributed to the soft internal structure of the helical PDMS stent, which makes it less prone to damage from bending and stretching during use, the helical structure sample used in the experiment has an initial length of 4 cm and a mass of 1.47 g. Before and after each experiment, we weighed and measured the samples. The results indicated that the samples were hardly damaged during the tests, and the lateral length remained stable due to their shape memory properties (Fig. 3e).

The stent designed in this study is intended to be wrapped around the physician's finger in order to collect real-time data within a constructed simulated vaginal environment (Fig. 4a). This method not only transforms the physician's subjective assessment of the simulated vaginal conditions into more objective and intuitive data, but also enhances diagnostic accuracy by utilizing changes in the stent's electrical resistance and the electromyographic signals induced by the physician's finger. Specifically, the stent's electrical resistance changes upon contact with the skin, and the accompanying muscle activity provides relevant physiological signals, offering more precise support for clinical diagnosis.

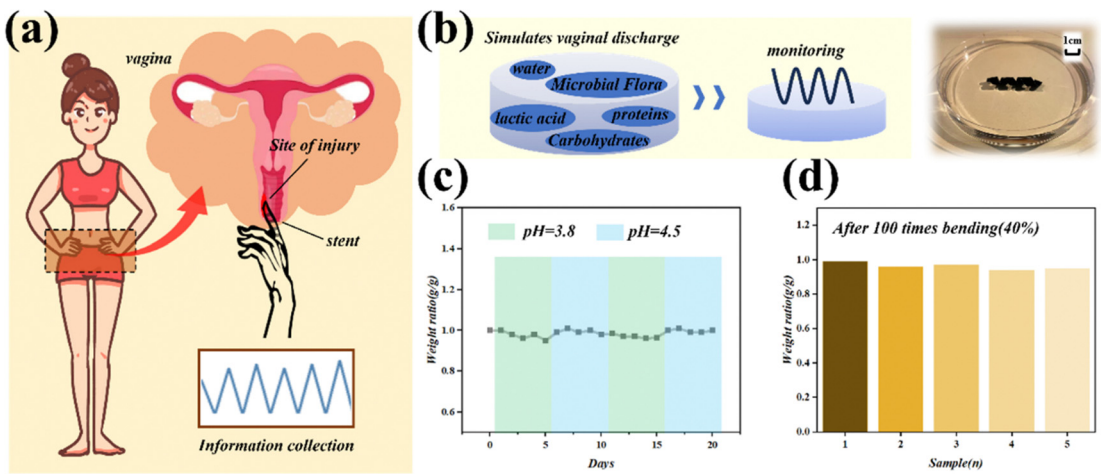

Fig. 4 The stent can be wrapped around a physician's finger for gathering real-time clinical data during examinations. (a) Schematic diagram of stent-assisted vaginal examination; (b) schematic and actual images of monitoring stent-assisted vaginal examination in a simulated vaginal fluid, demonstrating the feasibility of the stent in assisting examination within the vaginal environment; (c) integrity testing of the stent under two pH thresholds representative of vaginal conditions; (d) demonstration of the stent's ability to maintain structural integrity after multiple bending cycles.

To assess the biocompatibility of the stent within a vaginal environment, a simulated vaginal environment was constructed for experimental evaluation (Fig. 4b). This system incorporated biological materials such as water, lactic acid, and proteins, and adjusted the pH and temperature of the simulated fluid to closely mimic the physiological conditions of the human vaginal environment. During the experiment, the stent was placed in this simulated environment to observe and record its behavior under various pH and temperature conditions. Over a 20-day period, the performance and degradation of the stent were tested under two common pH thresholds representative of vaginal conditions (Fig. 4c). The results demonstrated that the stent maintained stable performance with negligible degradation. This indicates that the effect of pH on the durability of the stent is minimal and can be considered negligible.

To further assess the mechanical stability of the stents in specific use, we subjected the samples to the previously constructed simulated vaginal environment, bending the samples 100 consecutive times at a 40-degree angle to test their durability and structural integrity during repeated bending (Fig. 4d). The results revealed that all five samples exhibited minimal loss or structural deformation after the bending tests, indicating that the PDMS stent has excellent mechanical stability for long-term use.

Based on these experimental results, it can be inferred that this PDMS stent is highly feasible and stable as an auxiliary tool for vaginal examination in clinical applications. In summary, through systematic testing of the stent's biocompatibility and mechanical performance, this chapter validates the PDMS stent's excellent adaptability in the vaginal environment and its potential as an auxiliary diagnostic tool, providing both theoretical and experimental support for the future development of related medical devices.

In addition, we can use the inherent electrical conductivity of the stent to gather information about the bending deformation of the stent. We wrapped the helical PDMS stent around a medical catheter and conducted bending tests at different angles (Fig. 5a). During the preparation process, we incorporated a certain amount of carbon nanotubes into the base PDMS mixture, endowing it with excellent electrical conductivity. Subsequently, we bent the medical catheter at three different angles to achieve precise bending of the stent. When the stent was stationary, its relative resistance remained stable; however, when the stent began to bend, its relative resistance started to change, while the CNT-free stent exhibits almost no relative resistance change regardless of bending (Fig. 5b). At three different bending angles, the relative resistance exhibited the same pattern: each bending event produced a peak in relative resistance, and the magnitude of this peak increased with larger bending angles (Fig. 5c). This information transmission capability allows us to effectively monitor the bending state of a finger wrapped with the helical PDMS stent in real-time. To collect more comprehensive bending information, we also conducted bending cycle tests between two angles, specifically between 10° and 25° and between 25° and 40°. The observed relative resistance change patterns were consistent with the results from the aforementioned experiments (Fig. 5e). We utilized the structural color on the outer surface of the stent to record the changes in the peak wavelength of reflection during the 0° to 40° bending cycles (Fig. 5f), which can also be used to monitor the deformation of the stent. Therefore, by tracking the relative resistance changes of the helical PDMS stent, we can accurately perceive the stent's deformation, thereby monitoring the movement status of the finger.

In this study, we continued to test and discuss the application of the helical PDMS stent in postoperative finger rehabilitation. In the experiment, we used a set of EMG signal testing equipment, consisting of electrodes, sensors, a microcontroller, and Arduino software. This setup effectively recorded the EMG

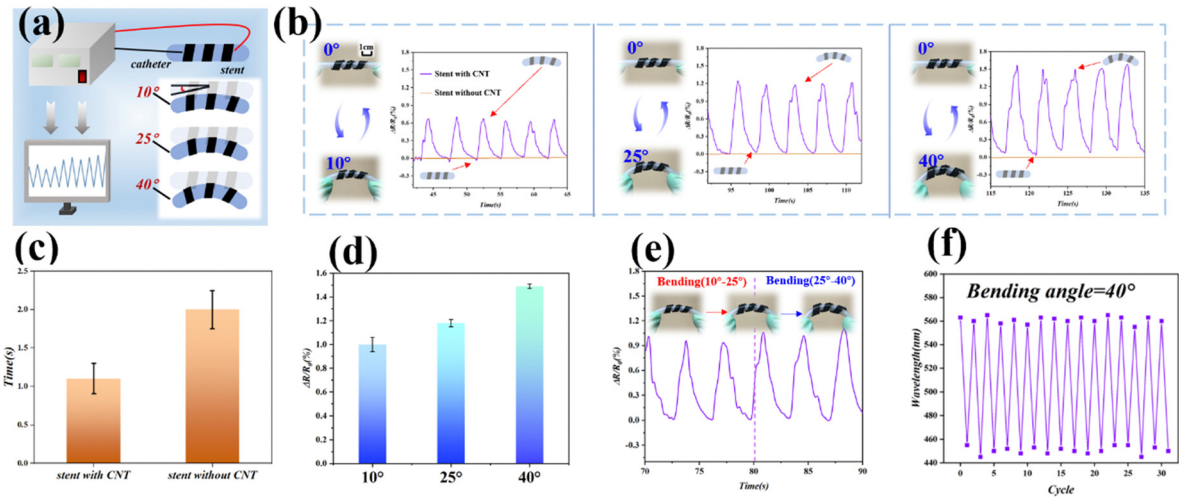

Fig. 5 Bending state monitoring of the stent. (a) Schematic diagram of the bending monitoring experiment; (b) changes in the relative resistance of the CNT-containing stent and CNT-free stent during cyclic bending tests at different angles (10°, 25°, 40°); (c) the time required for the CNT-containing stent and CNT-free stent to return to their initial forms after being stretched to maximum deformation; (d) comparison of relative resistance changes of the stent at three different bending angles; (e) changes in the relative resistance of the stent during cycles from 10° to 25° and from 25° to 40°; (f) changes in the structural color reflection peak of the film during the 40° bending cycle test.

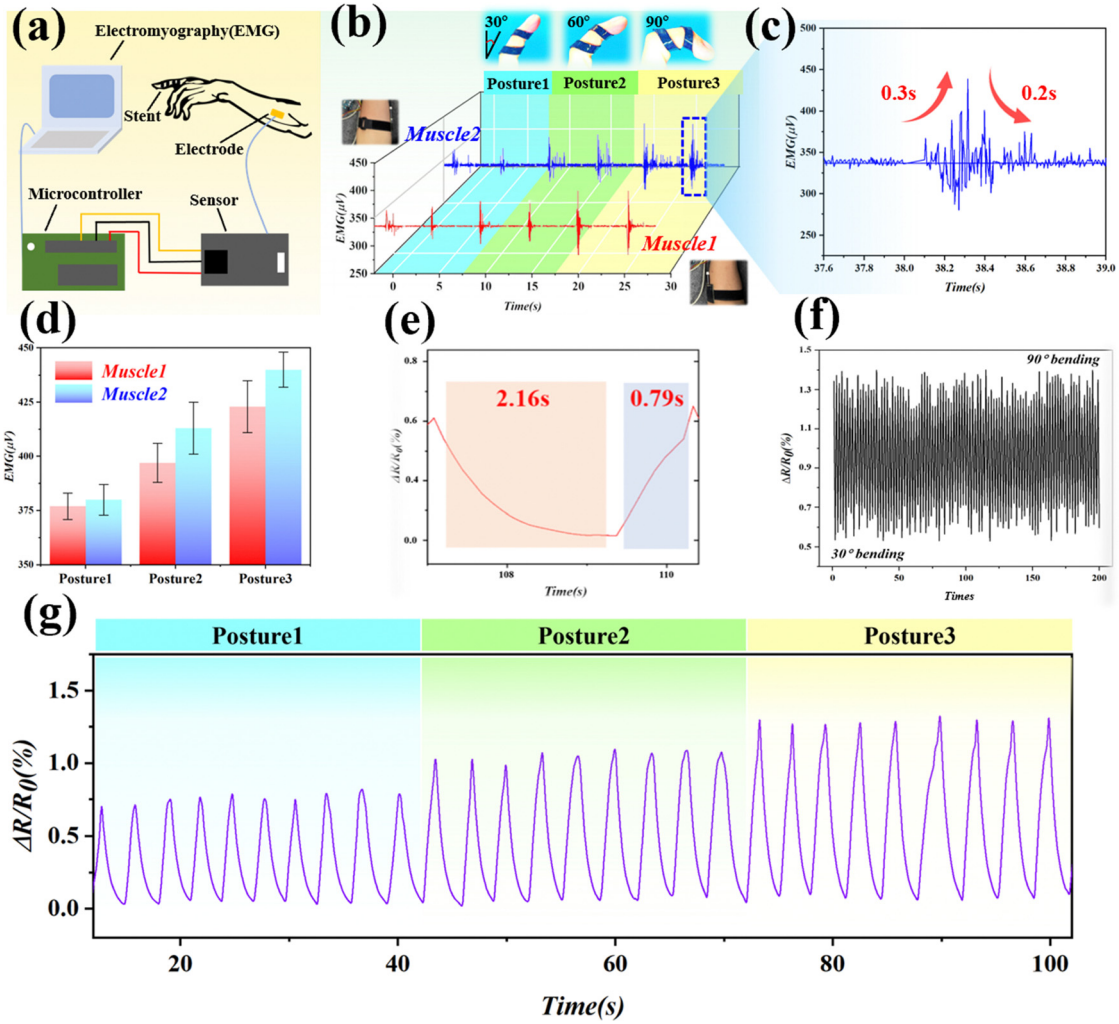

Fig. 6 Monitoring of finger motion. (a) Schematic diagram of the collection of EMG signals generated by finger movements; (b) EMG recordings from two arm muscles at different bending angles (30°, 60°, 90°) (muscle 1: extensor carpi ulnaris, muscle 2: flexor carpi radialis); (c) demonstration of a single motion waveform; (d) comparison of peak EMG signal values from the two muscles at three different bending angles; (e) sensitivity testing of the stent; (f) stability testing of the stent; (g) changes in the relative resistance of the stent at three different bending angles.

signals of the muscles corresponding to finger movements (Fig. 6a). We attached the electrodes to the extensor carpi ulnaris and the flexor carpi radialis muscles, as these muscles are more affected by finger movements. After connecting the equipment, we first kept the finger stationary until the EMG signals stabilized. We then bent the finger at three different angles (30°, 60°, 90°). The EMG signal changes varied with different bending angles, with larger angles causing more significant changes in the EMG signals (Fig. 6b). This is similar to the previous test results of the relative resistance changes of the helical PDMS stent. The waveform of the EMG signals produced by a single bend showed that the changes in EMG signals induced by finger movements were real-time and significant, with the waveform rising and falling within a very short time (Fig. 6c). This indicates that monitoring finger movements through EMG signals is highly feasible. Additionally, compared to the flexor carpi radialis muscle, the extensor carpi ulnaris muscle exhibited more pronounced EMG changes induced by finger movements (Fig. 6d), making the extensor carpi ulnaris more suitable for monitoring finger bending. This pattern corresponded well with the previous test results of resistance changes, where the relative resistance changes of the stent increased with larger bending angles (Fig. 6g). In the test, even with a small bending angle (4–5°), we were able to measure a very obvious change in the relative resistance value (Fig. 6e), which also verified that our scaffold has high sensitivity. This degree of sensitivity is already fully applicable to our clinical application scenario. Then we found that during 200 cycles, the relative resistance change induced by bending at specific angles remains stable, and the sample worked normally and still maintained good stability (Fig. 6f). The experimental results demonstrated that the idea of using the helical PDMS stent to assist in postoperative finger rehabilitation is feasible. By further studying the stability, thermally responsive properties, and shape memory of the helical PDMS stent, we aim to explore its potential applications in the sensor field.

Conclusion

In the field of gynecological medicine, the development of precise diagnostic and therapeutic modalities is of utmost importance. Bionics, which involves mimicking natural biological structures, has emerged as a promising approach. This study presents a helical PDMS scaffold inspired by the deformability of vines. The scaffold was fabricated using a sandwich thermoplastic method to produce hydrogel fibers with shape memory, thermal responsiveness, and deformation sensing. It also incorporates sensors for real-time monitoring and feedback. The Janus wettability of the hydrogel was achieved by depositing a silica monolayer structure film on the outer surface and adhering a PNiPAAm film to the inner surface, enhancing tissue interaction and stability. Mechanical studies demonstrated the scaffold's adjustable parameters and good mechanical performance, including stable stress–strain curves and resistance to damage from bending and stretching. Biocompatibility tests in a simulated vaginal environment showed minimal degradation and excellent adaptability. By monitoring the relative resistance changes of the helical PDMS stent, finger movement and deformation can be accurately perceived. Additionally, the study explored finger motion monitoring through sEMG signals, which corresponded well with the resistance change results. Overall, this research validates the potential of the helical PDMS scaffold as an auxiliary tool in gynecological examinations and surgeries, providing a theoretical foundation and practical applications for future innovations in gynecological diagnostics and surgical support.

Author contributions

Weipeng Lu and Qing He contributed equally to this work. Cihui Liu and Qian Dong conceived the idea and designed the experiment; Weipeng Lu, Qing He, Yue Cao and Zhiwei Jiang conducted experiments and wrote the paper. Sunlong Li, Weipeng Lu, Zheng Mao and Ying Wang analyzed the data. Songchao Fu, Yue Wang, Cihui Liu and Qian Dong took part in the discussion. All authors contributed to the preparation of the manuscript.

Statement of informed consent

Informed consent was obtained from all human participants prior to their involvement in this study. All experimental protocols were conducted in accordance with the Declaration of Helsinki.

Data availability

The data supporting this article have been included as part of the ESI.†

Conflicts of interest

There are no conflicts to declare.

Acknowledgements

This work was supported by funding from Shanghai Jiao Tong University.

References

1 A. Santoro, G. Angelico, A. Travaglino, F. Inzani, D. Arciuolo and M. Valente, *et al.*, New Pathological and Clinical Insights in Endometrial Cancer in View of the Updated ESGO/ESTRO/ESP Guidelines, *Cancers*, 2021, **13**(11), 2623.
2 J. García-Solares, J. Donnez, O. Donnez and M. M. Dolmans, Pathogenesis of uterine adenomyosis: invagination or metaplasia?, *Fertil. Steril.*, 2018, **109**(3), 371–379.
3 Z. Zhao, J. Kumar, Y. Hwang, J. Deng, M. S. B. Ibrahim and C. Huang, *et al.*, Digital printing of shape-morphing natural materials, *Proc. Natl. Acad. Sci. U. S. A.*, 2021, **118**(43), e2113715118.
4 N. Chen, M. Li, H. Wu, Y. Qin, J. Wang and K. Xu, *et al.*, An extracellular matrix-mimetic coating with dual bionics for cardiovascular stents, *Regener. Biomater.*, 2023, **10**, rbad055.
5 C. Zollfrank and C. Selhuber-Unkel, Recent Advances in the Field of Bioinspired Materials and Systems, *Adv. Funct. Mater.*, 2024, **34**(35), 2408945.
6 D. Li, T. Cui, J. Jian, J. Yan, J. Xu and X. Li, *et al.*, Lantern-Inspired On-Skin Helical Interconnects for Epidermal Electronic Sensors, *Adv. Funct. Mater.*, 2023, **33**(18), 2213335.
7 Y. Yu, F. Fu, L. Shang, Y. Cheng, Z. Gu and Y. Zhao, Bioinspired Helical Microfibers from Microfluidics, *Adv. Mater.*, 2017, **29**(18), 1605765.
8 Y. Gao, F. Guo, P. Cao, J. Liu, D. Li and J. Wu, *et al.*, Winding-Locked Carbon Nanotubes/Polymer Nanofibers Helical Yarn for Ultrastretchable Conductor and Strain Sensor, *ACS Nano*, 2020, **14**(3), 3442–3450.
9 M. Han, L. Chen, K. Aras, C. Liang, X. Chen and H. Zhao, *et al.*, Catheter-integrated soft multilayer electronic arrays for multiplexed sensing and actuation during cardiac surgery, *Nat. Biomed. Eng.*, 2020, **4**(10), 997–1009.
10 G. Arrick, D. Sticker, A. Ghazal, Y. Lu, T. Duncombe and D. Gwynne, *et al.*, Cephalopod-inspired jetting devices for gastrointestinal drug delivery, *Nature*, 2024, **636**, 481–487.
11 Z. Ji, C. Yan, B. Yu, X. Zhang, M. Cai and X. Jia, *et al.*, 3D Printing of Hydrogel Architectures with Complex and Controllable Shape Deformation, *Adv. Mater. Technol.*, 2019, **4**(4), 1800713.
12 G. Parada, Y. Yu, W. Riley, S. Lojovich, D. Tshikudi and Q. Ling, *et al.*, Ultrathin and Robust Hydrogel Coatings on Cardiovascular Medical Devices to Mitigate Thromboembolic and Infectious Complications, *Adv. Healthcare Mater.*, 2020, **9**(20), e2001116.
13 B. Liu, H. Li, F. Meng, Z. Xu, L. Hao and Y. Yao, *et al.*, 4D printed hydrogel scaffold with swelling-stiffening properties and programmable deformation for minimally invasive implantation, *Nat. Commun.*, 2024, **15**(1), 1587.

14 J. Wu, J. Xian, C. He, H. Lin, J. Li and F. Li, Asymmetric Wettability Hydrogel Surfaces for Enduring Electromyographic Monitoring, *Adv. Mater.*, 2024, **36**(41), 2405372.
15 X. He, D. Liu, B. Cui, H. Huang, S. Dai and I. Pang, *et al.*, Extreme Hydrogel Bioelectronics, *Adv. Funct. Mater.*, 2024, **34**(52), 2405896.
16 M. Wu, M. Pan, C. Qiao, Y. Ma, B. Yan and W. Yang, *et al.*, Ultra stretchable, tough, elastic and transparent hydrogel skins integrated with intelligent sensing functions enabled by machine learning algorithms, *Chem. Eng. J.*, 2022, 450.
17 W. Li, Q. Guan, M. Li, E. Saiz and X. Hou, Nature-inspired strategies for the synthesis of hydrogel actuators and their applications, *Prog. Polym. Sci.*, 2023, **140**, 101665.
18 D. Zhu, Z. Li, K. Huang, T. G. Caranasos, J. S. Rossi and K. Cheng, Minimally invasive delivery of therapeutic agents by hydrogel injection into the pericardial cavity for cardiac repair, *Nat. Commun.*, 2021, **12**(1), 1412.
19 M. Zhang, Y. Huang, W. Pan, X. Tong, Q. Zeng and T. Su, *et al.*, Polydopamine-incorporated dextran hydrogel drug carrier with tailorable structure for wound healing, *Carbohydr. Polym.*, 2021, **253**, 117213.
20 G. J. Rodriguez-Rivera, A. Post, M. John, S. Buchan, D. Bernard and M. Razavi, *et al.*, Injectable hydrogel electrodes as conduction highways to restore native pacing, *Nat. Commun.*, 2024, **15**(1), 64.
21 C. Hu, J. Zhou, J. Zhang, Y. Zhao, C. Xie and W. Yin, *et al.*, A structural color hydrogel for diagnosis of halitosis and screening of periodontitis, *Mater. Horiz.*, 2024, **11**(2), 519–530.
22 J. Wang, Y. Sun, P. Jia, J. Su, X. Zhang and N. Wu, *et al.*, Wearable nanocomposite hydrogel temperature sensor based on thermally-switchable and mechanical-deformation-insensitive structural colors, *Chem. Eng. J.*, 2023, **476**, 146602.
23 F. Gao, H. Jiang, D. Wang, S. Wang and W. Song, Bio-Inspired Magnetic-Responsive Supramolecular-Covalent Semi-Convertible Hydrogel, *Adv. Mater.*, 2024, **36**(29), e2401645.
24 C. Cui, T. Wu, X. Chen, Y. Liu, Y. Li and Z. Xu, *et al.*, A Janus Hydrogel Wet Adhesive for Internal Tissue Repair and Anti-Postoperative Adhesion, *Adv. Funct. Mater.*, 2020, **30**(49), 2005689.
25 J. Ren, X. Yin, Y. Chen, H. Su, K. Wang and L. Zhang, *et al.*, Alginate hydrogel-coated syringe needles for rapid haemostasis of vessel and viscera puncture, *Biomaterials*, 2020, **249**, 120019.
26 X. He, Z. Li, X. Huang, Q. Zhang, Y. Zeng and J. Li, *et al.*, Sweat-powered, skin-adhesive multimodal sensor for long-term and real-time sweat monitoring, *BMEMat*, 2024, e12124.
27 H. Lee, S. Lee, W. Lee, T. Yokota, K. Fukuda and T. Someya, Ultrathin Organic Electrochemical Transistor with Non-volatile and Thin Gel Electrolyte for Long-Term Electrophysiological Monitoring, *Adv. Funct. Mater.*, 2019, **29**(48), 1906982.
28 X. Qu, S. Cheng, Y. Liu, Y. Hu, Y. Shan and R. Luo, *et al.*, Bias-Free Cardiac Monitoring Capsule, *Adv. Mater.*, 2024, **36**(33), 2402457.
29 Y. F. Chen, Y. Zhou, L. H. Zhang, Y. Cao, S. L. Li and W. P. Lu, *et al.*, Bioinspired colloidal crystal hydrogel pressure sensors with Janus wettability for uterus cervical canal tension perception, *J. Mater. Chem. B*, 2024, **12**(36), 8941–8951.
30 L. Zhang, L. Ren, Y. Chen, Y. Cao, S. Li and W. Lu, *et al.*, An Octopus-Inspired Stimulus-Responsive Structural Color Hydrogel for Uterus Cervical Canal Stent, *Adv. Healthcare Mater.*, 2024, e2400439.
31 L. H. Zhang, L. H. Ren, S. L. Li, M. L. Xiong, Y. Cao and Y. F. Chen, *et al.*, A water strider-inspired intestinal stent actuator for controllable adhesion and unidirectional biofluid picking, *Mater. Today Bio*, 2024, **28**, 101216.
32 Z. Liu, J. Liu, Y. Bai, S. Wu, J. Zhao and L. Ren, A Bio-Inspired Janus Patch for Treating Abdominal Wall Defects, *Adv. Funct. Mater.*, 2024.
33 Y. Yang, T. Xu, H. P. Bei, Y. Zhao and X. Zhao, Sculpting Bio-Inspired Surface Textures: An Adhesive Janus Periosteum, *Adv. Funct. Mater.*, 2021, **31**(37), 2104636.
34 Y. Chen, W. Zheng, Y. Xia, L. Zhang, Y. Cao and S. Li, *et al.*, Implantable Resistive Strain Sensor-Decorated Colloidal Crystal Hydrogel Catheter for Intestinal Tract Pressure Sensing, *ACS Appl. Mater. Interfaces*, 2024, **16**(17), 21736–21745.
35 W. Lin, H. Zhang, W. Zhang, H. Qi, G. Zhang and J. Qian, *et al.*, *In vivo* degradation and endothelialization of an iron bioresorbable scaffold, *Bioact. Mater.*, 2021, **6**(4), 1028–1039.
36 J. Xue, C. Qin and C. Wu, 3D printing of cell-delivery scaffolds for tissue regeneration, *Regener. Biomater.*, 2023, **10**(6), 2056–3418.
37 Y. Yang, Y. Zhang, R. Chai and Z. Gu, A Polydopamine-Functionalized Carbon Microfibrous Scaffold Accelerates the Development of Neural Stem Cells, *Front. Bioeng. Biotechnol.*, 2020, **8**, 616.